Photoion rotational distributions from near-threshold to deep in the continuum

E. D. Poliakoff, Heung Cheun Choi, R. M. Rao, A. G. Mihill, Sandeep Kakar, Kwanghsi Wang, and V. McKoy

Citation: The Journal of Chemical Physics **103**, 1773 (1995); doi: 10.1063/1.469751
View online: http://dx.doi.org/10.1063/1.469751
View Table of Contents: http://scitation.aip.org/content/aip/journal/jcp/103/5?ver=pdfcov
Published by the AIP Publishing

Photoion rotational distributions from near-threshold to deep in the continuum

E. D. Poliakoff,[a),b)] Heung Cheun Choi,[a)] R. M. Rao,[b)] A. G. Mihill,[c)] and Sandeep Kakar[d)]
Louisiana State University, Baton Rouge, Louisiana 70803

Kwanghsi Wang and V. McKoy
Arthur Amos Noyes Laboratory of Chemical Physics,[e)] California Institute of Technology, Pasadena, California 91125

(Received 6 March 1995; accepted 24 April 1995)

We present the first measurements of ion rotational distributions for photoionization over an extended range [$0 \leqslant E_K \leqslant 200$ eV for N_2 ($2\sigma_u^{-1}$) and $3 \leqslant E_K \leqslant 125$ eV for CO ($4\sigma^{-1}$)]. The N_2 ion rotational distributions are seen to change dramatically over this energy range, indicating that characteristically molecular behavior of the photoelectron persists far from ionization threshold. In addition, the N_2 and CO results show a strikingly different dependence on energy. Although differences are expected due to the absence of a center of symmetry in CO, detailed calculations reveal that this behavior arises from the presence of Cooper minima in the $2\sigma_u \rightarrow k\sigma_g$ continuum in the case of N_2 and from an f-wave shape resonance in the $4\sigma \rightarrow k\sigma$ channel in CO. Agreement between measured and calculated ion rotational distributions is excellent. The N_2 results are also compared with electron bombardment ionization data. This comparison demonstrates that previous interpretations of electron bombardment data are prone to errors. © *1995 American Institute of Physics.*

I. INTRODUCTION

Rotationally resolved photoion distributions can provide significant insight into the underlying dynamics of molecular photoionization, one of the simplest of molecular fragmentation processes.[1–29] As in all fragmentation processes, determination of the final state distributions of the fragments provides a window on the electronic and nuclear motion of the collision complex responsible for the asymptotic fragment distributions. In photoionization, the collision complex consists of the photoelectron and ion core and rotationally resolved photoelectron spectra hence serve as a probe of electron–core interactions at short range. These rotationally resolved spectra have highlighted significant dynamical features such as the coupling of angular momentum in molecular photoelectrons and the effects of shape resonances[23–26] and Cooper minima.[27–29] Furthermore, many studies have illustrated the effectiveness of a strong interplay between theory and experiment in analysis of such spectra.

While there have been widespread and successful efforts to probe rotationally resolved aspects of photoionization, work to date has been geared primarily towards understanding the rotational dynamics in the threshold or near-threshold region. Extension of such studies to higher photoelectron energies can potentially display dynamical behavior which may not be apparent from near-threshold studies. In this paper, we report the first study of rotationally resolved photoionization with a sufficient scope to discern such trends in the ionization dynamics. Specifically, we compare the rotationally resolved photoionization of N_2 and CO, where the photoelectron kinetic energy is varied from $0 \leqslant E_K \leqslant 200$ eV for N_2 and $3 \leqslant E_K \leqslant 125$ eV for CO. Previous rotationally resolved work has typically been restricted to $E_K \leqslant 1$ eV, so the present study expands the accessible range by 2 orders of magnitude. This is significant because dynamical features can extend over tens of electron volts, so studies which can survey trends over comparable ranges are quite useful. A preliminary report of the present study has been published elsewhere.[29] This paper describes the investigation in detail. The N_2 and CO systems, although isoelectronic and chemically similar in many respects, exhibit striking differences in their photoelectron dynamics which only become apparent when the range of the rotationally resolved studies is extended far from threshold. The ability to compare the rotational dynamics for these systems over a wide range is made possible by the experimental method, namely, dispersed fluorescence from electronically excited photoions. This strategy has been effectively exploited for related vibrationally resolved studies.[30–32] The current work is part of a larger program aimed at discerning molecular aspects of the photoionization dynamics over a wide spectral range by probing uniquely molecular signatures of these processes.

It has long been recognized that rotationally resolved photoionization provides insight into the coupling of electronic and nuclear motion. While dipole selection rules constrain the angular momentum of the photoelectron–photoion complex, the partitioning of angular momentum between the electron and ion is governed by the ionization dynamics.[5–13,29,33–47] Conservation of angular momentum dictates that the change in core angular momentum is restricted by[10]

$$\Delta J = J^+ - J_0 = (l+3/2),(l+1/2),\ldots,-(l+3/2). \quad (1)$$

[a)]Department of Chemistry.
[b)]Department of Physics.
[c)]Center for Advanced Microstructures and Devices.
[d)]Present address: HASYLAB, DESY, D22603 Hamburg, Germany.
[e)]Contribution No. 9055.

 0021-9606/95/103(5)/1773/15/$6.00

Excluding electron spin, the change in angular momentum, ΔN, is hence given by

$$\Delta N = N^+ - N_0 = (l+1), l, \ldots, -(l+1). \quad (2)$$

Thus for an $l=3$ photoelectron (i.e., an f wave), changes in the ion core angular momentum as large as $\Delta J = 9/2$ are possible (or, $\Delta N = 4$). Note that interference between partial waves can play an important role in determining the intensity of each rotational transition. The angular momentum composition of the photoelectron can be strongly energy dependent and this is why data that span a wide range of energies are particularly useful.[24,26,29,30,47]

The requirement of extensive spectral coverage presents a serious obstacle for studying rotational distributions in molecular photoionization. To emphasize how demanding this goal is, consider the following constraints. Energy spacings between adjacent rotational levels, even for favorable diatomic systems, are on the order of 4 cm^{-1} (500 *micro*volts). Spectral features of interest persist to photon energies—and photoelectron kinetic energies—in excess of 200 eV, as we will demonstrate. Hence, to achieve rotational resolution at 200 eV, resolving powers in excess of 10^6 are required. This is many orders of magnitude beyond the limits of the highest resolution photoelectron spectroscopy at comparable energies.[48–50] Thus dispersed fluorescence measurements can generate insights into the rotationally resolved photoionization dynamics at high energies that are otherwise inaccessible.

To place the current study into context, it is useful to review other methods for obtaining rotationally resolved data. The earliest experiments were high-resolution photoelectron spectroscopy measurements of H_2 using resonance lamp excitation.[1,4,51] Hydrogen was chosen as the target system (in part) because the rotational spacings are large, enabling rotationally resolved photoelectron spectroscopy with achievable energy resolution ($\Delta E \approx 15$ meV). This scheme of resonance lamp vacuum ultraviolet excitation coupled with photoelectron spectroscopy has been restricted mainly to studies of hydrogen close to threshold. There have been extensions enabling studies of other molecules using deconvolution methods,[52] but these studies are similarly restricted to low photoelectron energies and fixed resonance lamp excitation energies.

Many recent advances have been achieved via innovations with lasers and photoelectron spectroscopy. For example, some studies combine resonance enhanced multiphoton ionization with photoelectron spectroscopy (REMPI-PES).[5,6,34–36,41–46] Because rotational resolution usually exceeds the limits of conventional photoelectron spectroscopy, two approaches have been used. One method is to select H_2 or another diatomic hydride with a large rotational constant.[5,41–43,45,46] Another technique is to use the first stage of the REMPI process to state-select a high-N level, so that the spacings between adjacent rotational levels are comparatively large and can be resolved via time-of-flight photoelectron spectroscopy.[6,34–36] These REMPI-PES strategies exploit laser technology to go beyond the limits of earlier resonance lamp studies. They enable studies of systems other than H_2, as well as some tuning of the photoelectron kinetic energy. However, the REMPI/PES strategy is limited to studies near the ionization threshold, owing to constraints on the energy range accessible with lasers and resolution limits for high-energy electrons.

An elegant experimental advance related to the REMPI-PES strategy is the REMPI-LIF combination (i.e., REMPI coupled to laser induced fluorescence) developed by Zare and Xie.[11,12,33] A central point demonstrated in their studies is that properly designed optical probes can offer much higher resolution than photoelectron spectroscopic techniques. They exploited this advantage to determine the population of individual Λ-doublet components of molecular ions. Like REMPI-PES studies, REMPI-LIF work is restricted to near-threshold studies. However, these studies demonstrate the inherent advantage in resolution that optical probes exhibit *vis-à-vis* photoelectron spectroscopy.

Finally, the method which is currently most widely used is zero-kinetic-energy, pulsed-field-ionization (ZEKE-PFI) photoelectron spectroscopy.[10,15–21,40,52–62] This method was pioneered by Müller–Dethlefs[15,54] and White,[10,53] and has been applied to the widest variety of systems. Many other groups, including those of Grant,[17,55,57,60,61] Softley,[16,56] Hepburn,[18] Knee,[62] Gerber,[63] and Weisshaar[64] have used ZEKE-PFI for spectroscopic and dynamical studies. By exploiting the continuity of oscillator strength across the ionization threshold, field ionization of extremely high Rydberg states (i.e., $n \geqslant 150$) is used to extract ''pseudophotoelectron'' spectra. While ZEKE-PFI offers the possibility of studying the widest variety of systems, it is restricted to threshold photoionization.

We demonstrate that rotationally resolved data can be generated over the necessary range by detecting dispersed fluorescence from excited photoions, confirming the technical advantages that have been illustrated in other high resolution studies.[29,31,37] Because we observe fluorescence, *the detection bandwidth is uncoupled from, and therefore not limited by, the excitation bandwidth*,[31,65–67] permitting us to exploit the broad tunability of synchrotron radiation. Figure 1 depicts the experimental strategy in a diagrammatic form, comparing the detection of energy analyzed photoelectrons with energy analyzed ionic fluorescence. This ''cartoon view'' illustrates that the lower limit of the photoelectron energy resolution is the energy bandwidth of the photon source, which is typically quite broad relative to rotational spacings when synchrotron radiation is used as the excitation source. On the other hand, the fluorescence bandwidth is determined solely by the optical system (i.e., the dispersion and slit width for the fluorescence monochromator), so dispersed fluorescence has the key advantage of accessing highly resolved data on the photoion when the excitation bandwidth is broad and tunability is critical. Earlier studies have demonstrated that the method yields useful and reliable results. In particular, the earlier work also shows that the results are free of artifacts such as valence–electron cascades that might complicate the interpretation of the data.[31]

The approach of using dispersed fluorescence detection for studies requiring broad spectral coverage has been described in many related contexts, including studies of Franck–Condon breakdown in shape resonant ionization of

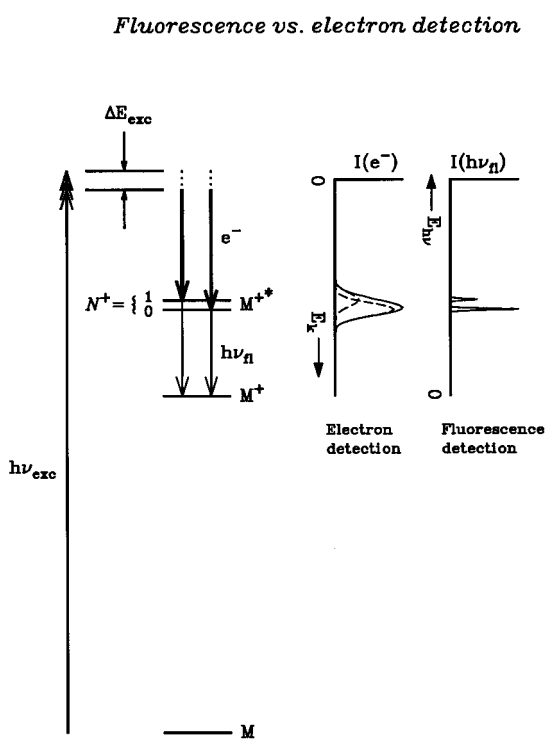

FIG. 1. This comparison between photoelectron spectroscopy and fluorescence spectroscopy as probes of molecular photoionization illustrates that the detection bandwidth of the fluorescence method is not limited by the excitation bandwidth.

diatomics,[65,68] triatomics,[66,67,69] and polyatomics.[70] The strategy employed in those studies—probing the ionic vibrational degrees of freedom to elucidate the scattering dynamics—is closely related to the present rotationally resolved studies. In particular, a central message common to all of these studies is that probing molecular aspects of the ionization process (i.e., rotation, vibration, alignment) provides a window on microscopic details of the photoelectron dynamics. The current study demonstrates that the molecular aspects and even the chemically specific aspects persist far from the ionization threshold.

II. EXPERIMENTAL DETAILS

The experimental method has been described previously[31,32,65] and is reviewed briefly here. A schematic of the apparatus is shown in Fig. 2. Synchrotron radiation from the Louisiana State University, Center for Advanced Microstructures and Devices (CAMD) facility,[71] is monochromatized ($\Delta h\nu_{\mathrm{exc}} \approx 0.5$ eV) by a 6 m plane grating monochromator (PGM)[72] and ionizes the target molecules. The electron beam energy is 1.3 GeV, and typical stored beams are 100 mA. Under these conditions, the photon flux incident on the target molecules is 10^{12} s^{-1}. As we will show, it is necessary to acquire large data sets and the data accumulation takes extended periods. The availability of beam time at CAMD and the flexibility of the PGM beam line are key factors that make the experiments possible.

The procedures for performing these measurements are similar to those described elsewhere.[31,32] The synchrotron radiation is channeled to the interaction region using a two-stage capillary (2 mm inner diameter) differential pumping section (not shown in Fig. 2). This maintains the ultrahigh vacuum integrity of the beam line ($\sim 10^{-9}$ Torr) and electron storage ring, while allowing the experimental chamber to be maintained at comparatively high pressure ($\sim 8\times 10^{-4}$ Torr). The main chamber is pumped by a 2500 L/s cryopump (CTI model CT-10). It is useful to limit the number of target states, so a free-jet supersonic expansion is used to rotationally cool the target molecules.[73] A 50 μm diameter nozzle was used with a stagnation pressure $P_s = 15$ atm. The nozzle was partially plugged, but the orifice size was constant, as the chamber pressure was constant for a given stagnation pressure. Data were obtained over a range of stagnation pressures to test for secondary processes, such as ionization induced by secondary photoelectrons.

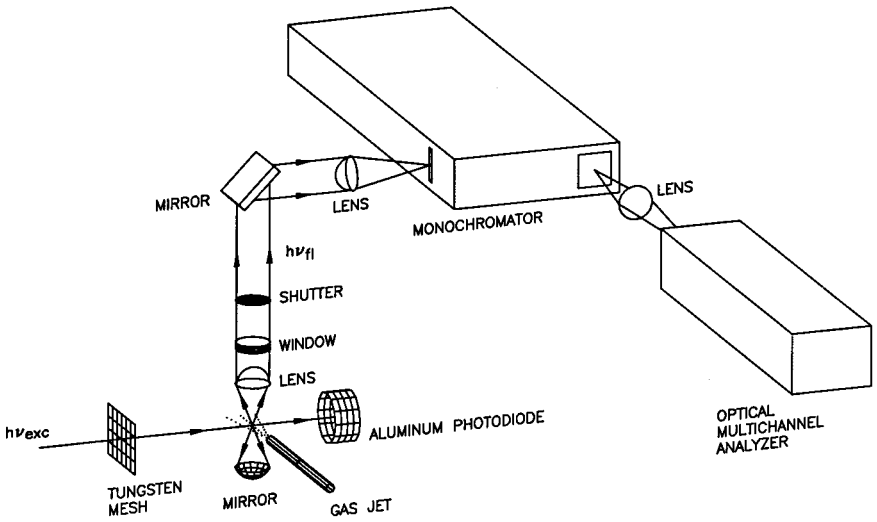

FIG. 2. Experimental schematic.

The excitation and fluorescence sequence is the same as used previously,[8,37,65] i.e., neutral N_2 molecules are photoionized and the dispersed fluorescence, $h\nu_{N^+N''}$, is monitored. The excitation-fluorescence sequence for N_2 is

$$\begin{aligned} &N_2(X\ ^1\Sigma_g^+, v_0=0, \{N_0\}) + h\nu_{\rm exc} \\ &\quad \rightarrow N_2^+(B\ ^2\Sigma_u^+, v^+=0, N^+) + e^- \\ &\qquad \downarrow \\ &\quad N_2^+(X\ ^2\Sigma_g^+, v''=1, N'') + h\nu_{N^+N''}. \end{aligned} \tag{3}$$

Because there are two lower levels in these studies (i.e., the neutral target level in the ionization transition and the lower level of the ionic fluorescence transition), we use the convention of the double-prime superscript to denote a lower level in the fluorescence transition, and a 0 subscript indicates a target level undergoing ionization. The notation $\{N_0\}$ denotes that the target rotational levels undergoing ionization are not selected. The target levels are sufficiently restricted by the supersonic cooling that the interpretation is not unduly complicated. Similarly, N^+ indicates the nascent ionic levels of the $N_2^+(B\ ^2\Sigma_u^+)$ excited ionic state. The CO measurements are analogous, as the molecules are isoelectronic. The only difference is that the g/u subscript is absent because of the lack of an inversion center.

The experiments on CO are difficult, as the fluorescence intensity is comparatively low and the resolution requirement is demanding. The separations between several adjacent fluorescence transitions are less than 0.3 Å. For this reason, the experimental apparatus was upgraded from our previous fluorescence apparatus. The present experiments utilize a 1 m fluorescence monochromator (Instruments SA model THR-1000) rather than the smaller one used previously.[8,37,65] Using a 3600 g/mm grating, the reciprocal linear dispersion is 1.5 Å/mm at 4275 Å and 2.4 Å/mm at 2300 Å. The entrance slit width of the fluorescence monochromator is set to 300 μm for N_2 and 80 μm for CO, resulting in bandwidths $\Delta\lambda$ of 0.45 and 0.19 Å, respectively. Another change from previous experiments is that the channel plate-based optical multichannel analyzer (Quantar Technology, model 2601A) is mounted axially, rather than laterally with respect to the monochromator axis. A biconvex lens is used to project the monochromator focal plane onto the OMA detector plane. We do not employ a photomultiplier tube detector in these studies.

The N_2 data were generated over the range $20 \leqslant h\nu_{\rm exc} \leqslant 220$ eV. Fluorescence spectra were obtained at least every 5 eV. At lower energies, a finer energy mesh was used. The signal intensities were lower for CO and results were obtained from $23 \leqslant h\nu_{\rm exc} \leqslant 145$ eV with fluorescence spectra at 10 eV intervals for the highest energies.

III. THEORY AND NUMERICAL DETAILS

A. Theory

The formulation of rotationally resolved photoionization used here has been described elsewhere.[22,74] We briefly review the necessary background and highlight those aspects that are pertinent for interpretation of the dispersed fluorescence measurements. As this discussion will show, all of the major theoretical and computational machinery for interpreting these experiments is already in place. The calculations were simply performed over a wider spectral range than for previous studies to obtain the ion distributions needed for comparison with the present experiments.

The cross section for ionization of a J_0 level of the initial state to a J^+ level of the ion, $\sigma(J_0 \rightarrow J^+)$, can be written as

$$\sigma(J_0 \rightarrow J^+) \propto \sum_{\substack{lm \\ M_{J_0} M_{J^+}}} \rho_{M_{J_0} M_{J_0}} |C_{lm}(M_{J_0}, M_{J^+})|^2, \tag{4}$$

where $\rho_{M_{J_0} M_{J_0}}$ is the population of the M_{J_0} sublevel of the initial state and the coefficients $C_{lm}(M_{J_0}, M_{J^+})$ are related to the probability for photoionization of the magnetic M_{J_0} sublevel leading to the M_{J^+} sublevel of the ion. For a Σ–Σ transition of interest here, both initial and ionic states can be best described by the Hund's case (b) coupling scheme and $C_{lm}(M_{J_0}, M_{J^+})$ has the simple form[22,74]

$$\begin{aligned} C_{lm}(M_{J_0}, M_{J^+}) = C'_{lm} \Bigg[\sum I_{l\lambda\mu} \begin{pmatrix} N^+ & N_0 & N_t \\ -\Lambda_+ & \Lambda_0 & \lambda_t \end{pmatrix} \\ \times \begin{pmatrix} N_t & 1 & l \\ -\lambda_t & \mu & -\lambda \end{pmatrix} \Bigg], \end{aligned} \tag{5}$$

with

$$I_{l\lambda\mu} = (-i)^l e^{i\eta_l} \int dR\ \chi^*_{v^+}(R) r^{l\lambda\mu}_{fi}(R) \chi_{v_0}(R), \tag{6}$$

where C'_{lm} are the laboratory-frame quantities, χ is the vibrational wave function, $I_{l\lambda\mu}$ is the vibrationally averaged photoelectron matrix element between the initial state and the photoelectron continuum wave function, η_l is the Coulomb phase shift, N_t is the angular momentum transfer, m and λ are the projections of l in the laboratory and molecular frames, respectively, μ is the photon polarization index in the molecular frame, and R denotes its dependence on internuclear distance. From the properties of 3-j symbols, it is easy to obtain the parity selection rules from Eq. (5)

$$N^+ - N_0 + l = \text{odd}. \tag{7}$$

The constant implied by the proportionality in Eq. (4) is unimportant for our present purposes and is dropped in subsequent expressions.

Since the fluorescence experiment integrates over all initial rotational levels J_0, we consider all the transitions terminating in a specific ion level J^+, i.e.,

$$n_{J^+} = \sum_{J_0} \sigma(J_0 \rightarrow J^+). \tag{8}$$

The relative populations $\rho_{M_{J_0} M_{J_0}}$ of Eq. (4) are governed by the supersonic expansion conditions. In our calculations, the initial J_0 rotational levels are assumed to be unaligned, i.e., all M_{J_0} sublevels of the J_0 level are equally populated. The rotational temperatures for N_2 and CO expansions are assumed to be 14 and 18 K, respectively. These temperatures are determined by fitting to the experimental data, analogous to the procedures used when comparing single-photon

ZEKE-PFI experiments to theory.[53,58] Spin statistics are considered in determining the rotational populations of N_2.

The degree of rotational excitation in the photoionization process is strongly influenced by the angular momentum composition of the photoelectron. As a result, a key quantity is the photoelectron matrix element, $r_{fi}^{l\lambda\mu}(R)$ of Eq. (6), from a bound orbital ϕ_i into a continuum orbital $\phi_{f,\mathbf{k}}^{(-)}(\mathbf{r},R)$, where $\mathbf{k}$ is the momentum of the photoelectron and $(-)$ denotes incoming-wave boundary conditions appropriate to photoionization. The partial wave components $\psi_{klm}^{(-)}$ of $\phi_{f,\mathbf{k}}^{(-)}(\mathbf{r},R)$ are obtained by an expansion about $\hat{\mathbf{k}}$,

$$\phi_{f,\mathbf{k}}^{(-)}(\mathbf{r},R)=(2/\pi)^{1/2}\sum_{lm} i^l\psi_{klm}^{(-)}(\mathbf{r},R)Y_{lm}^*(\hat{\mathbf{k}}). \tag{9}$$

Single-center expansions of $\psi_{klm}^{(-)}(\mathbf{r},R)$ and $\phi_i(\mathbf{r}',R)$, e.g.,

$$\psi_{klm}^{(-)}(\mathbf{r},R)=\sum_{l'\lambda} g_{l,l'\lambda}(k,r,R)\mathscr{D}_{m\lambda}^{l}Y_{l'\lambda}(\hat{\mathbf{r}}'), \tag{10}$$

define partial wave photoelectron matrix elements in the molecular frame for ionization of orbital $\phi_i(\mathbf{r}')$, i.e.,

$$r_{fi}^{l\lambda\mu}(R)=\sum_{l',l_0}\langle g_{l,l'\lambda}(k,r,R)Y_{l'\lambda}(\hat{\mathbf{r}}')|rY_{1\mu}(\hat{\mathbf{r}}')|\phi_{l_0} \times(r,R)Y_{l_0\lambda_0}(\hat{\mathbf{r}}')\rangle. \tag{11}$$

The $\mathscr{D}_{m\lambda}^{l}$ in Eq. (10) is a rotational matrix in Edmonds' notation.[75] Whereas only $l=l'$ terms would be allowed in Eq. (11) for the central fields of atomic systems, where the angular momentum of the photoelectron must be conserved, $l\neq l'$ terms arise in molecules due to angular momentum coupling brought about by the nonspherical molecular ion potential. These l-changing collisions strongly influence the ion rotational distributions in molecular photoionization. This point has been discussed in REMPI-PES studies[5,6,41–43] and ZEKE-PFI investigations[10,40,76] and is even more important in the context of these energy-dependent studies. The present fluorescence measurements allow us to see how this underlying dynamical behavior evolves with energy.

B. Final state wave functions

There are two dipole-allowed channels for photoionization of the $2\sigma_u$ and 4σ orbitals of the ground state N_2 and CO, respectively. An electron from these orbitals can be ejected into the $k\sigma_g(k\sigma)$ or $k\pi_g(k\pi)$ continuum channel. Ionization into the $k\sigma_g(k\sigma)$ and $k\pi_g(k\pi)$ continua results in an electron–ion complex of $^1\Sigma_u^+(^1\Sigma^+)$ and $^1\Pi_u(^1\Pi)$ total final-state symmetries, respectively. The final-state wave functions for N_2 (similarly for CO) are

$$\Psi(^1\Sigma_u^+)=\frac{1}{\sqrt{2}}\left[|(\text{core})2\sigma_u\overline{k\sigma_g}|-|(\text{core})\overline{2\sigma_u}k\sigma_g|\right] \tag{12}$$

and

$$\Psi(^1\Pi_u^+)=\frac{1}{\sqrt{2}}\left[|(\text{core})2\sigma_u\overline{k\pi_g}|-|(\text{core})\overline{2\sigma_u}k\pi_g|\right], \tag{13}$$

where $(\text{core})=1\sigma_g^2 2\sigma_g^2 3\sigma_g^2 1\sigma_u^2 1\pi^4$.

Within the frozen-core Hartree–Fock approximation, the one-electron Schrödinger equation for the photoelectron orbital ψ_{klm} associated with the wave functions of Eqs. (12) and (13) can be shown to be of the form[77,78]

$$P\left(f+\sum_{i=\text{core}}(2J_i-K_i)+a_nJ_n+b_nK_n-\epsilon\right)P|\psi_{klm}\rangle=0, \tag{14}$$

where J_i and K_i are the Coulomb and exchange operators, respectively, and P is a projection operator which enforces orthogonality of the continuum orbital to the occupied orbitals.[77,78] The photoelectron kinetic energy is given by $\epsilon=(1/2)k^2$ and the one-electron operator f is

$$f=-\frac{1}{2}\nabla_i^2-\sum_{\alpha}\frac{Z_\alpha}{r_{i\alpha}}, \tag{15}$$

with Z_α a nuclear charge. Using the wave functions of Eqs. (12) and (13), the coefficients a_n and b_n associated with the $2\sigma_u$ and 4σ orbitals assume values of 2 and 1, respectively.

To obtain the photoelectron orbitals we have used an iterative procedure, based on the Schwinger variational principle,[77,78] to solve the Lippmann–Schwinger equation associated with Eq. (14). In this procedure, the static-exchange potential of the ion is approximated by

$$\mathbf{U}(\mathbf{r},\mathbf{r}')=\sum_{ij}\langle\mathbf{r}|\mathbf{U}|\alpha_i\rangle(U^{-1})_{ij}\langle\alpha_j|\mathbf{U}|\mathbf{r}'\rangle, \tag{16}$$

where the matrix $\mathbf{U}^{-1}$ is the inverse of the matrix with element $(U)_{ij}=\langle\alpha_i|\mathbf{U}|\alpha_j\rangle$ and the α's are discrete basis functions such as Cartesian or spherical Gaussian functions. $\mathbf{U}$ is twice the static-exchange potential in Eq. (14) with the long-range Coulomb potential removed. The Lippman–Schwinger equation with this separable potential $\mathbf{U}(\mathbf{r},\mathbf{r}')$ can be readily solved and provides approximate photoelectron orbitals $\psi_{klm}^{(0)}$. These solutions can be iteratively improved to yield converged solutions to the Lippmann–Schwinger equation containing the exact static-exchange potential.

C. Numerical details

The process has thus far been considered implicitly at the independent-particle level. Our calculations are performed at the Hartree–Fock level, which is sufficient to identify and account for the key dynamical aspects. The ground state wave functions of N_2 and CO are obtained at the self-consistent-field (SCF) level. The Gaussian basis functions for both molecules are the same as in Ref. 18. A single-center expansion of the $2\sigma_u$ orbital of N_2 around the center of mass gives 90.65% p, 6.66% f, and 1.52% h ($l_0=5$) character at the equilibrium internuclear distance of $R_e=2.0743$ a.u. This $2\sigma_u$ orbital changes its composition slowly from 96.86% p and 2.62% f character at an internuclear distance of 1.25 a.u. to 81.52% p and 11.30% f character at $R=3.5$ a.u. The angular momentum composition of the 4σ orbital of CO is 14.56% s, 62.35% p, 15.67% d, 3.09% f, 2.72% g ($l_0=4$), 0.36% h ($l_0=5$), and 0.57% i ($l_0=6$) at $R_e=2.1322$ a.u. It is interesting to note that this 4σ orbital has considerable amount of even component, especially the s and d partial waves due to the lack of the center of symmetry in contrast

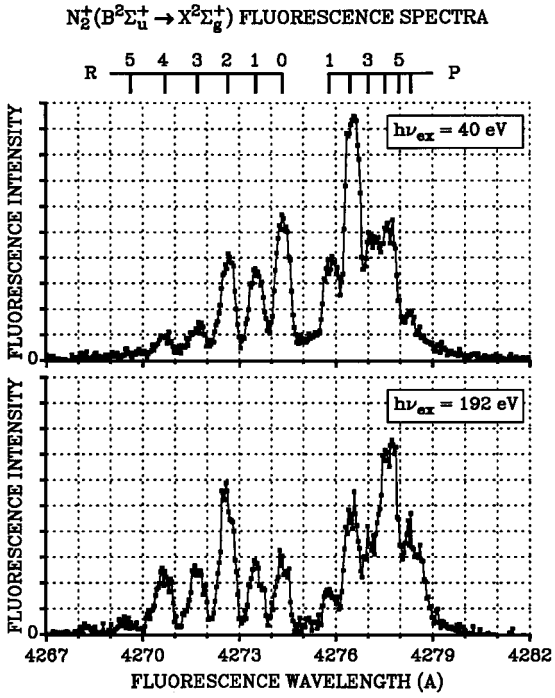

FIG. 3. Rotationally resolved fluorescence spectra of N_2^+ ($B\ ^2\Sigma_u^+$, $v^+=0$) photoions.

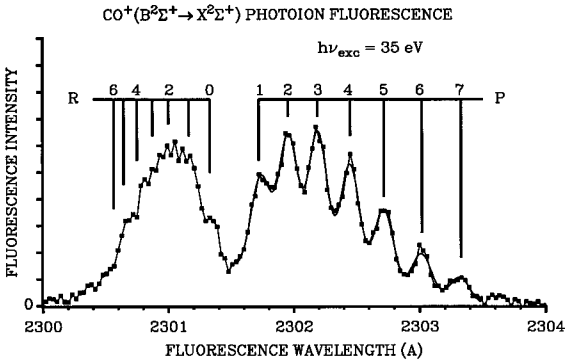

FIG. 4. Rotationally resolved fluorescence spectra of CO^+ ($B\ ^2\Sigma^+$, $v^+=0$) photoions.

to the corresponding $2\sigma_u$ orbital of the isoelectronic molecule N_2, which has only odd partial waves. This 4σ orbital also evolves differently from the $2\sigma_u$ orbital of N_2 with internuclear distance. For example, it has a dominant s, p, and d composition at small internuclear distance (29.76% s, 43.55% p, 23.60% d, 1.04% f, 1.62% g ($l_0=4$), 0.12% h ($l_0=5$), and 0.18% i ($l_0=6$) at $R=1.5$ a.u.), a dominant p character at $R=2.6$ a.u. [11.93% s, 71.83% p, 5.51% d, 4.75% f, 2.70% g ($l_0=4$), 0.62% h ($l_0=5$), and 0.96% i ($l_0=6$)], and a dominant s and p admixture at larger internuclear distance (19.84% s, 60.37% p, 5.82% d, 6.45% f, 1.49% g ($l_0=4$), 0.84% h ($l_0=5$), and 1.11% i ($l_0=6$) at $R=3.5$ a.u.).

For the final state, we assume a frozen-core Hartree–Fock model in which the ion orbitals are taken to be those of the ground states of N_2 and CO and the photoelectron orbital is obtained as a solution of a one-electron Schrödinger equation of Eq. (14). All matrix elements arising in the solution of the Lippmann–Schwinger equation were evaluated via single-center expansions at the center of mass.

IV. RESULTS AND DISCUSSION

A. Overview

Figure 3 shows two examples of photoion fluorescence spectra for N_2^+ ($B\ ^2\Sigma_u^+ \rightarrow X\ ^2\Sigma_g^+$), one obtained at low energy ($h\nu_{\rm exc}=40$ eV) and one at high energy (192 eV). The intensities of transitions originating from alternative rotational levels of the ion are dramatically different. This indicates that the photoion rotational distributions are changing with photon energy, or alternatively stated, the rotational transitions depend strongly on the photoelectron kinetic energy over a broad range. A $CO^+(B\ ^2\Sigma^+ \rightarrow X\ ^2\Sigma^+)$ fluorescence spectrum is shown in Fig. 4 and the rotational transitions are partially resolved. Only one CO^+ spectrum is shown because the relative intensities of the transitions do not change substantially with energy as they do in the N_2^+ spectra.

To extract the rotational distributions, we determine the population of each N^+ level, n_{N^+}, from the relative fluorescence intensities, as described previously,[37,79] i.e.,

$$n_{N^+}=K(2N^++1)I_{N^+N''}/S_{N^+}, \tag{17}$$

where K is a constant and S_{N^+} is a Hönl–London factor.[80] For R-branch transitions, $S_{N^+}=N^+$, and for P-branch transitions, $S_{N^+}=N^++1$. The R-branch transitions have larger separations than those of the P-branch in the N_2 spectra, so we use the R-branch transitions for extracting the populations (i.e., the n_{N^+}) where possible. It is necessary to get information on the $N^+=0$ level from the P-branch, since the lowest ionic rotational level in R-branch is $N^+=1$ [i.e., the $R(0)$ line]. We determine the $N^+=0$ population from the $P(1)$ fluorescence intensity. For the CO spectra, the P-branch transitions have greater resolutions than those of the R-branch, so all populations are extracted from the P-branch intensities. To compare data taken at different energies, we report the normalized ionic rotational populations ($n_{N^+}/\Sigma n_{N^+}$).

The bar graph in Fig. 5 shows a small subset of the $N_2^+(B\ ^2\Sigma_u^+)$ population data to provide an overview of the dependence of the photoion rotational distributions on energy. The pattern exhibited in Fig. 5 is striking and qualitatively revealing. The $N_2^+(B\ ^2\Sigma_u^+)$ rotational distributions change dramatically with energy. As the photon energy is increased, the populations of lower rotational levels are decreasing, those of the higher rotational levels are increasing, and the intermediate levels show comparatively little change. In other words, population is shifting from low N^+ levels to higher ones with increasing energy, indicating that larger ΔN ionization transitions increase with energy. For the weakly populated $N^+=5$ and 6 levels, the relative populations increase by more than a factor of 4, while the $N^+=1$ population falls by a factor of 2. These results can be understood if we assume that low ΔN transitions (i.e., $\Delta N=\pm 1$) dominate at lower photon energies, while larger ΔN transitions (i.e.,

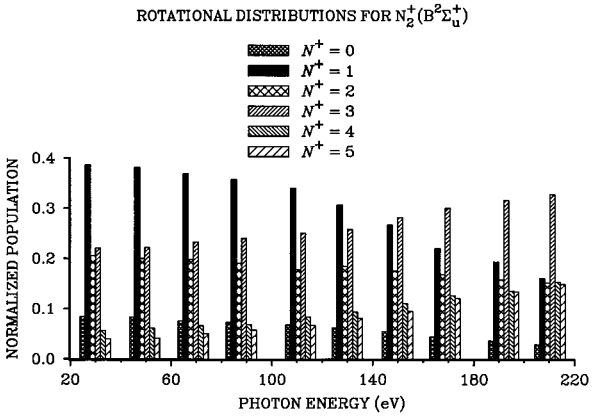

FIG. 5. Bar graph showing N_2^+ ($B\ ^2\Sigma_u^+$, $v^+=0$) rotational populations vs $h\nu_{\rm exc}$.

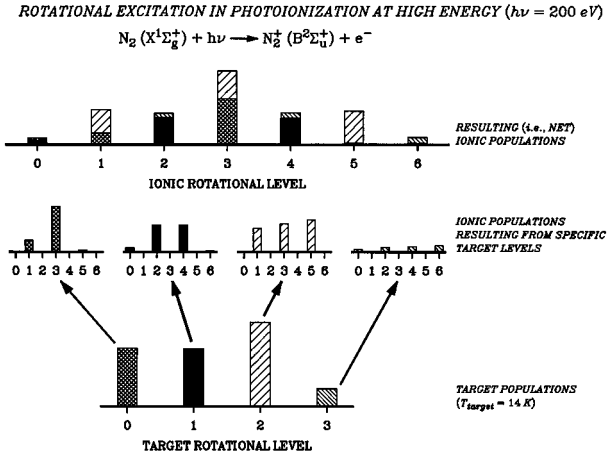

FIG. 6. A graphical description of how rotational distributions are calculated. The target molecules are assumed to be at a rotational temperature of 14 K. The state resolved processes are shown in the middle frames and the net ionic distribution is shown in the top of bar graph. The photon energy is 200 eV.

$|\Delta N|\geqslant 3$) grow in importance as the photon energy is increased. These trends are due to changes in angular momentum coupling between the photoelectron and the ion core.[58] The selection rule constrains ΔN to be odd ($\Delta N=\pm1,\pm3,\pm5,\cdots$), owing to the inversion symmetry of N_2.[9,22]

The data are not corrected for differences in rotational alignments. While it is possible to include alignment effects in the present treatment, both theory and experiment demonstrate that the influence is very slight,[81–85] especially at the higher energies employed in the current study.[84,85] The alignment provides a useful complementary probe, particularly for the high energy region, and is the topic of related fluorescence polarization studies.[84,85]

In a simplistic view, Fig. 5 shows that the ions are becoming ''hotter'' with increasing photon energy. Note that temperature is not a valid description of the ionic population distribution, as the photoions do not constitute an equilibrium ensemble. Nonetheless, it is sometimes useful to characterize the distributions using temperature as a parameter, as described previously.[37,86,87] We will defer the parametrization of the data by an effective rotational temperature until later.

To understand the trends exhibited in Fig. 5, it is useful to represent the theoretical results graphically for a specific photon energy. The process of distributing population from target to ionic rotational levels is illustrated step by step in Fig. 6 for $h\nu_{\rm exc}\approx200$ eV. The bottom bar graph denotes the relative populations of the target molecules, assuming $T_0=14$ K. Only the lowest four rotational target levels are populated appreciably, which simplifies the interpretation. (The 2:1 intensity alternation is due to nuclear spin statistics.) Each bar graph in the middle section of Fig. 6 shows the *calculated* ion populations for photoionization of a specific target level. The top graph of Fig. 6 shows the net ion rotational populations for photoionization of all four target levels, which are the quantities that can be measured by experiment. The stacking of each bar in the top frame allows one to trace the calculated parentage of each ion level to a particular target level. At the photon energy of Fig. 6, both $\Delta N=3$ and $\Delta N=\pm1$ transitions occur with appreciable intensities. The $\Delta N=3$ transition from the $N_0=2$ level leads to a significant population of the $N^+=5$ level. Of course, a $\Delta N=1$ transition from $N_0=4$ level could also populate the $N^+=5$ level, but this mechanism is not significant because the population of the $N_0=4$ level is so small. The resulting (i.e., net) ion populations shown in the top diagram of Fig. 6 indicate that the populations of 4, 5, and 6 levels of N_2^+ result mainly from $\Delta N=3$ transitions. This simple illustration demonstrates that information approaching state-to-state clarity can be extracted by exploiting physical constraints.

Figure 6 is also useful for describing and comparing the information content of different types of rotationally resolved photoionization measurements. The top frame shows the net population of each ion rotational level. This is appropriate for comparison with fluorescence data as the net ion populations can be extracted from the rotationally resolved fluorescence intensities. On the other hand, a conventional single-photon photoelectron or pseudo-photoelectron spectrum, such as ZEKE-PFI, provides populations of the individual transitions shown in the middle frame of Fig. 6. As for an ionic fluorescence spectrum, the relative intensities for the transitions in such photoelectron spectra are temperature-dependent because the initial target populations depend on temperature. This dependence has not presented any obstacles in the analysis of these spectra and we will show that it presents no difficulties in the ionic fluorescence studies either. Finally, resonance enhanced multiphoton ionization measurements go one step further by state selecting the target level for photoionization. Thus REMPI-PES, REMPI-LIF, and REMPI-PFI simplify the measurement by state selecting a single frame from the middle of Fig. 6. The calculations needed for comparison with any of these measurements are identical, emphasizing a central point of this analysis. Namely, the dynamical aspects of the calculations do not require a particular target state (or states). *Knowing the intensity of any single transition is sufficient to determine any other transition intensity via a geometrical transformation that contains no dynamical information*. The pertinent part of the calculation is contained in the dipole amplitudes

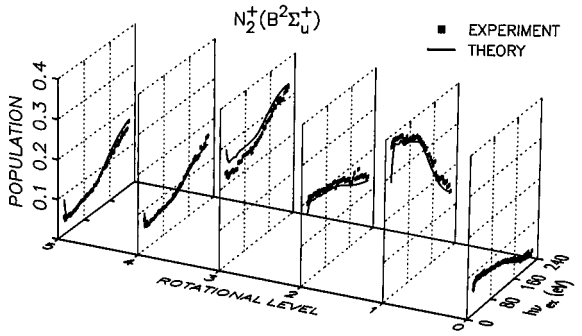

FIG. 7. N_2^+ ($B\ ^2\Sigma_u^+$, $v^+=0$) rotational populations vs $h\nu_{\rm exc}$.

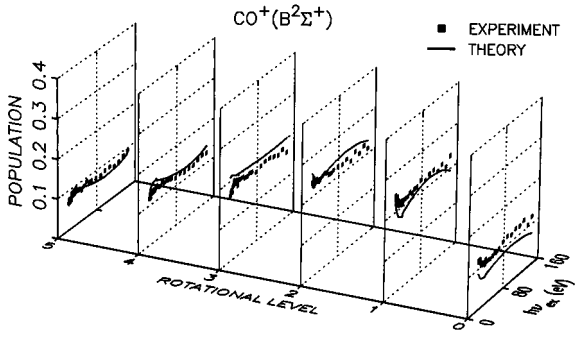

FIG. 8. CO^+ ($B\ ^2\Sigma^+$, $v^+=0$) rotational populations vs $h\nu_{\rm exc}$.

for the various partial waves, as described in Sec. III A. [This can be verified by examining the right-hand side of Eqs. (4)–(11) and noting that they are independent of N_0, N^+, and ΔN.] The primary goal of the experiment is to provide information on the partial wave composition, which ultimately yields insights into microscopic aspects of electron ion–core collisions. There are cases when it can be advantageous to determine the intensities of specific $N_0 \rightarrow N^+$ transitions and these have been discussed at length.[9,13,19,53] In the present study, the fluorescence measurements provide considerable insight and sufficient detail into the angular momentum transfers that occur during the ionization process. As a result, the data yield information on the energy-dependent angular momentum composition of the photoelectron matrix element with great clarity.

The complete experimental and theoretical data sets for N_2 are shown in Fig. 7. The calculated results have only one adjustable parameter, the temperature of the neutral target molecules (assumed to be 14 K for N_2). The rotational distributions continue to change at photon energies as high as 220 eV, the highest energy measured and more than ten times the binding energy for this channel. Overall agreement between experiment and theory is excellent. While the data from Fig. 7 include the subset shown in Fig. 5, the denser energy mesh reveals an inflection point at approximately 120 eV for several of the N^+ subplots. This is a useful clue in understanding the underlying dynamics, as will be demonstrated below. Also, while the overall agreement is striking, experiment and theory diverge markedly in the near-threshold region. Note that the area of disagreement spans a region of more than 10 eV. While this is a comparatively minor part of the complete data set, it is precisely this area that is accessible from alternative methods. Moreover, the spectral extent of the discrepancy exceeds any previous rotationally resolved ionization studies. Features such as this threshold discrepancy and the high energy inflection (i.e., $h\nu_{\rm exc} \approx 120$ eV) reinforce the importance of generating data over a broad range in order to discern trends and unravel ionization dynamics. We will interpret these N_2 results below, but first it is useful to compare them to the CO data.

Figure 8 shows the CO data. The contrast with the N_2 results is surprising for these two isoelectronic systems. The CO distributions are much flatter than those of N_2. Agreement between theory and experiment is good, although not as striking as for N_2. The behavior of the rotational populations for CO between 25 and 50 eV arises from the $4\sigma \rightarrow k\sigma$ shape resonance, which has been observed in previous photoionization studies.[68,88,89] However, these new data enable us to study the shape resonant dynamics with greater clarity than previously possible. Rotationally resolved studies can be particularly valuable for understanding the microscopic behavior of shape resonances for two reasons. First, a shape resonant wave function has enhanced amplitude in the core region. Second, shape resonances are frequently characterized by a particular asymptotic l value and Eqs. (1) and (2) indicate that this permits considerable leverage on the degree of rotational excitation.

The data shown in Fig. 8 might lead one to assume that *small* ΔN transitions occur over the whole range studied for CO $4\sigma^{-1}$ photoionization. However, the data are consistent with another interpretation, namely, that *large* ΔN transitions are occurring over the whole energy range. Indeed, the results shown in the next section demonstrate that the actual explanation is the latter, namely, that large ΔN transitions are intense at low energy, and persist at higher energies. In order to demonstrate this, it is useful to show simple CO calculations in graphical form for high and low photon energies. This is done in Fig. 9 where the high and low energy predictions are seen to be similar. Both are characterized by large ΔN transitions, with $\Delta N=2$, 3, and 4 transitions showing strong intensities at high ($h\nu_{\rm exc}=200$ eV) and low ($h\nu_{\rm exc}=40$ eV) energies. The rotational temperature of the target molecules is assumed to be 18 K. Note that ΔN is not restricted to odd values, in contrast to N_2. N_2 results are shown at two energies in Fig. 10. The dominance of small ΔN transitions at low energy and large ΔN at high energy is in stark contrast to the CO results.

B. Partial wave composition and interpretation of the rotational distributions

In this section, we present a description of the N_2 and CO photoionization dynamics based on an examination of the partial wave composition of the photoelectron matrix element. For this purpose, it is helpful to focus our attention on a small subset of the data. Such a subset is shown in Fig. 11, where the energy dependences are given only for $n_{N^+=1}$ of N_2 and CO. The N_2 results show a gradual decrease from threshold to roughly 100 eV, followed by a rapid decrease

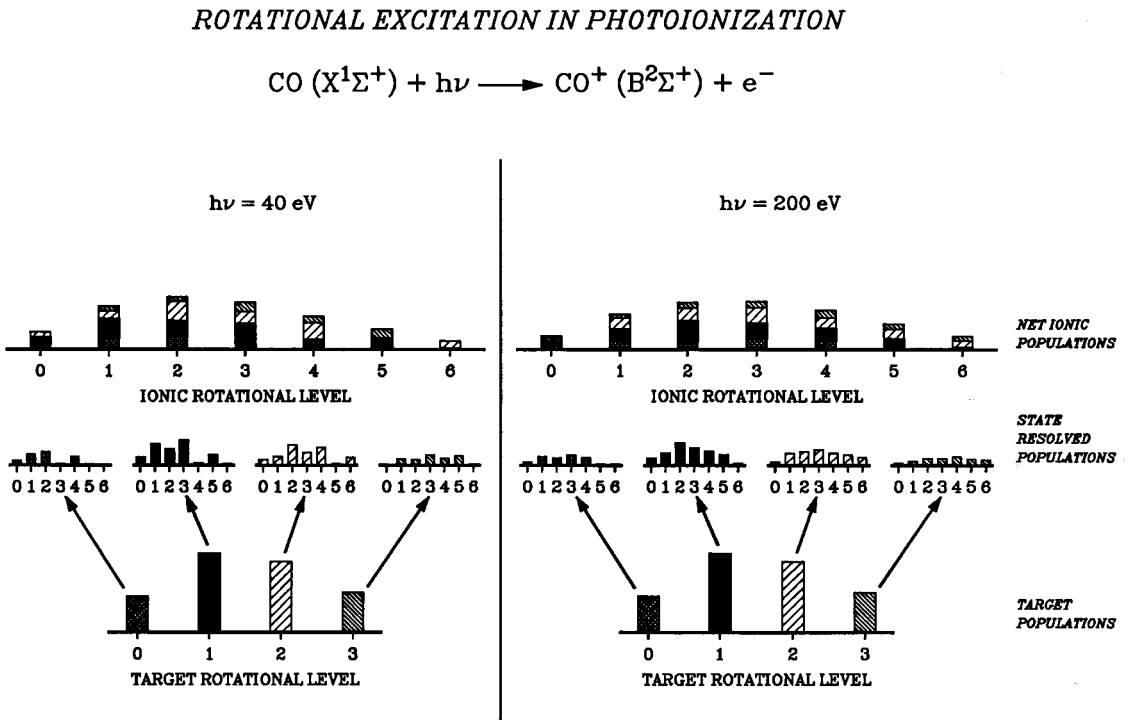

FIG. 9. Calculated rotational distributions for CO $4\sigma^{-1}$ photoionization at high and low energies. Note that the rotational distributions for the ion are similar and that $\Delta N=2$, 3, and 4 have appreciable intensity at both energies.

after approximately 130 eV. The extent of disagreement for the near-threshold N_2 distributions is also apparent in Fig. 11. The $n_{N^+=1}$ results for CO are qualitatively different from those of N_2 and, in particular, there is a broad dip from 20–50 eV, followed by a gradual recovery.

Figure 12 shows the calculated magnitudes $|D^{(-)}_{l\lambda\mu}|$ of the (incoming-wave, normalized) photoelectron matrix element for N_2 $(2\sigma_u^{-1})$ photoionization at the equilibrium internuclear

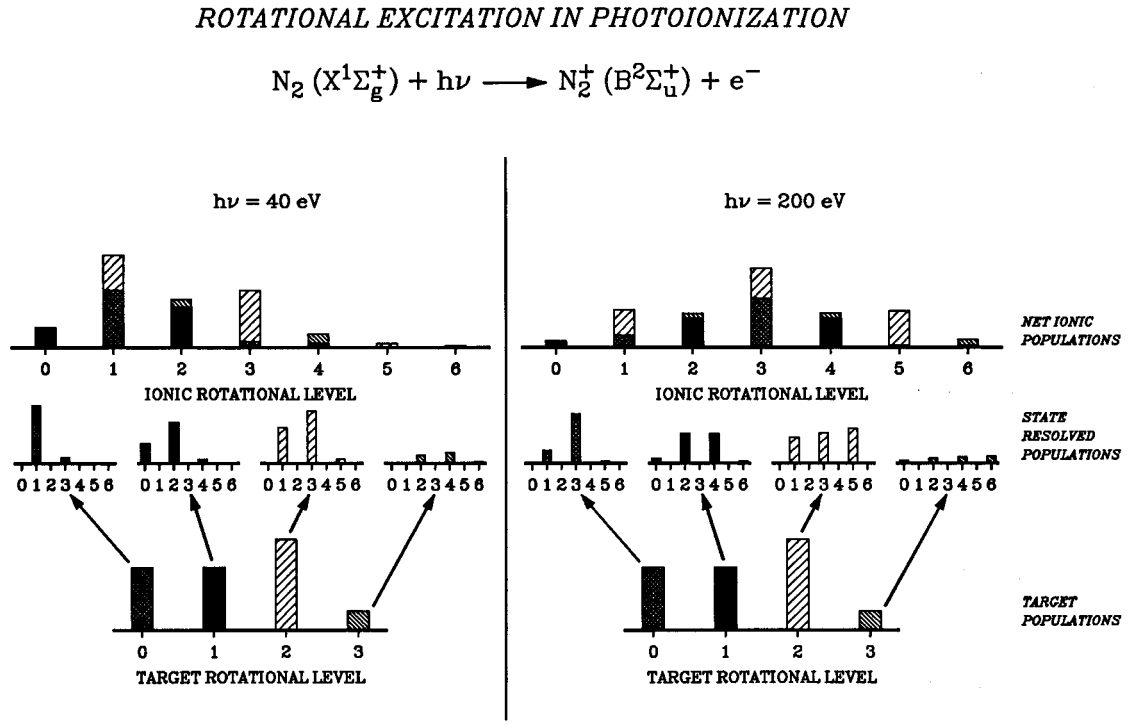

FIG. 10. Calculated rotational distributions for N_2 $2\sigma_u^{-1}$ photoionization at high and low energies. The rotational distribution at high energy is dramatically different from the one at low energy. At low energy, $\Delta N=\pm1$ transitions dominate, while $\Delta N=\pm3$ transitions are equally intense at the higher energy.

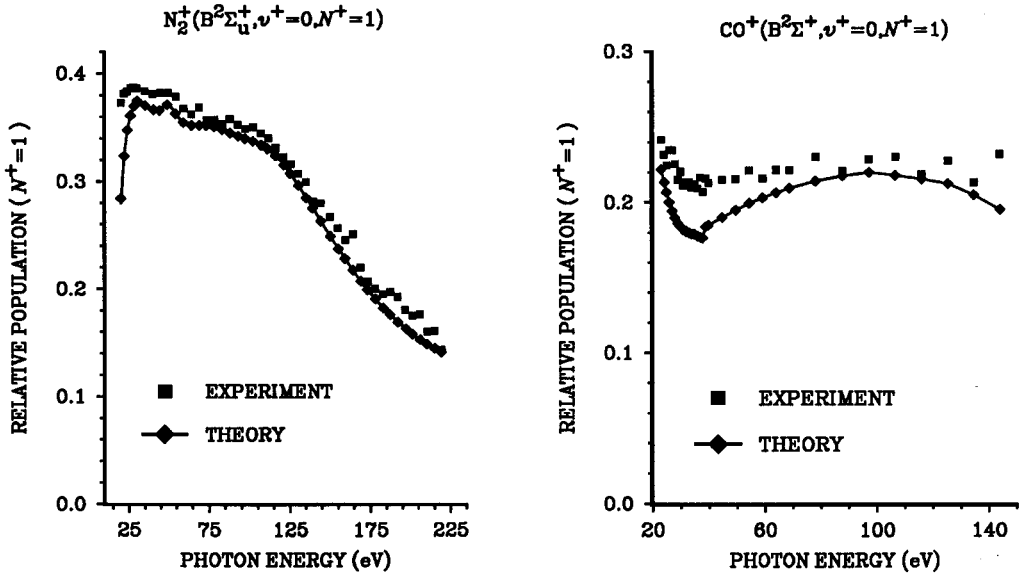

FIG. 11. Comparison of $N^+=1$ population curves for N_2^+ ($B\ ^2\Sigma_u^+$, $v^+=0$) and CO^+ ($B\ ^2\Sigma^+$, $v^+=0$) photoions.

distance of 2.0743 a.u. Note that the $D^{(-)}_{l\lambda\mu}$ here is one of the μ components of the $r_{fi}^{l\lambda\mu}(R)$ in Eq. (11). There are two symmetry-allowed channels, $2\sigma_u \rightarrow k\sigma_g$ and $2\sigma_u \rightarrow k\pi_g$. Only even l components are allowed, due to inversion symmetry. There is no $l=0$ component for the $2\sigma_u \rightarrow k\pi_g$ channel, as the $k\pi_g$ channel is restricted to l waves with $m_l=\pm 1$. Several features are notable. First, the l composition reflects the nonatomic dynamics of the photoelectron directly. As stated earlier, the $2\sigma_u$ orbital has mainly p (90.65%) character. There is no region where $\Delta l=\pm 1$ behavior dominates, which shows that the photoelectron is being rescattered by the anisotropic molecular field of the photoion [i.e., the $l \neq l'$ terms in Eq. (11)]. The results in Fig. 12 provide an explanation of the inflection point at $h\nu_{\mathrm{exc}} \approx 120$ eV. There are two l curves in the $2\sigma_u \rightarrow k\sigma_g$ continuum that exhibit strong minima, the $l=4$ curve at $h\nu_{\mathrm{exc}} \approx 100$ eV and the $l=2$ curve at $h\nu_{\mathrm{exc}} \approx 120$ eV. These strong dips are due to Cooper minima.[27] They lead to a suppression of high-l components of the photoelectron matrix element at low energy which are subsequently enhanced at higher energies. This results in the observed behavior of small ΔN transitions dominating at low energy and high ΔN transitions dominating at higher energies, with an inflection point in the region of the two Cooper minima. On the basis of the experimental data, it is not possible to assign the d or g wave as the component responsible for the observed inflection point.

The data in Fig. 12 also provide an explanation for the discrepancy between experiment and theory for photoionization of the $2\sigma_u$ level of N_2 in the threshold region. None of the l components in the $2\sigma_u \rightarrow k\pi_g$ channel have appreciable dipole strength near threshold. There is apparently something unusual about the $2\sigma_u \rightarrow k\pi_g$ channel, as previous theoretical results[78,90,91] also show poor agreement with other types of experimental data in this threshold region. All previous theoretical treatments have underestimated the dipole strength for the $k\pi_g$ channel near threshold. Presumably, there is intrac-

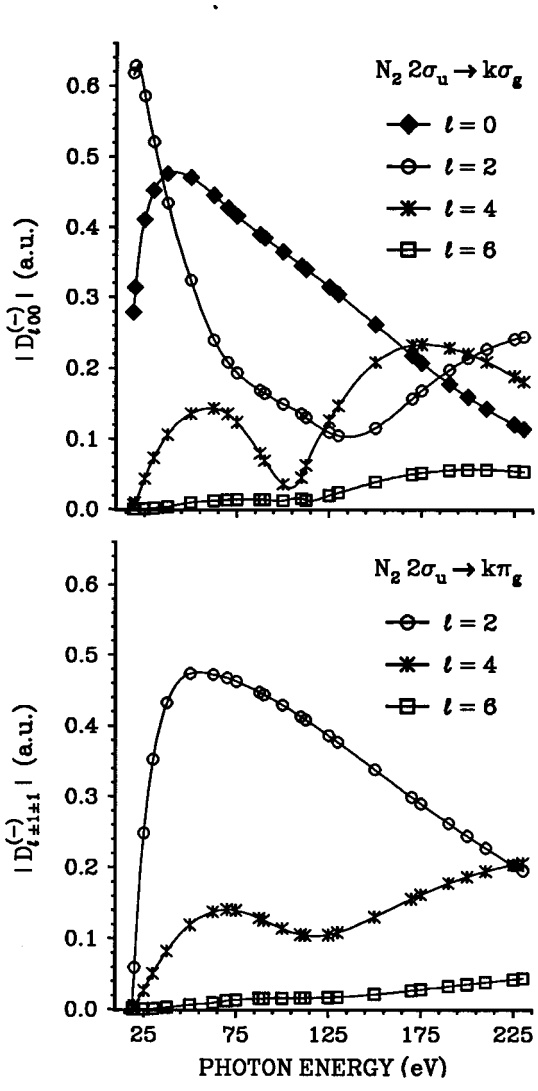

FIG. 12. Dipole strengths for N_2 photoionization.

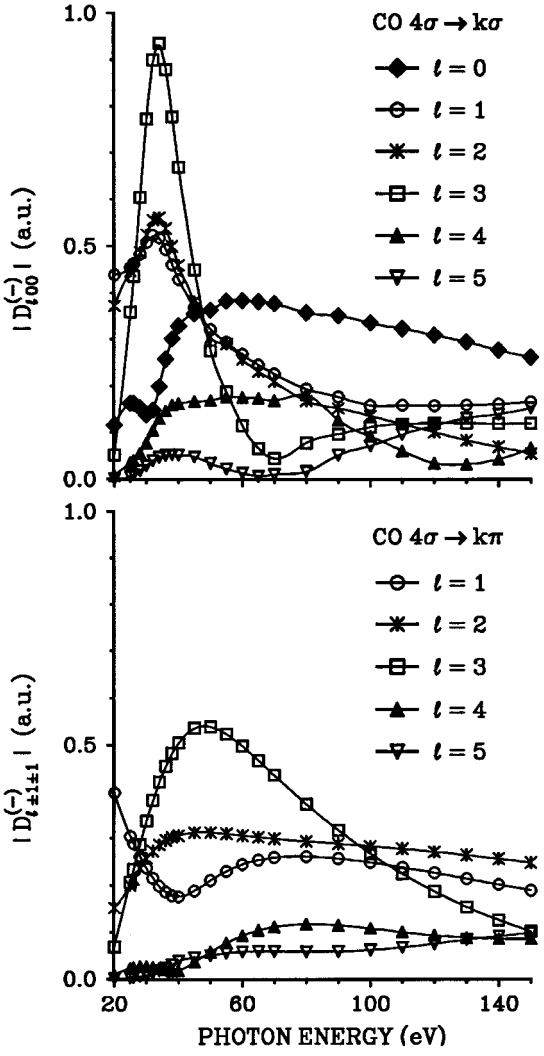

FIG. 13. Dipole strengths for CO photoionization.

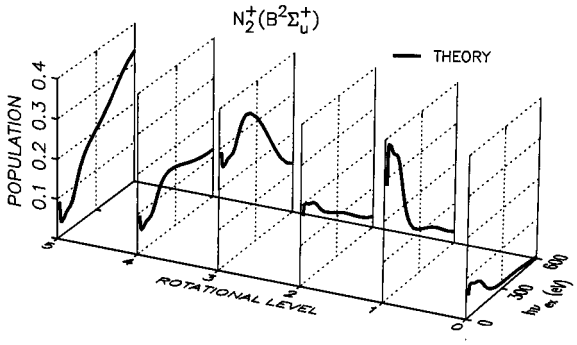

FIG. 14. Prediction for higher energy behavior for N_2.

hannel coupling (e.g., a strong autoionizing resonance in a $2\sigma_u \rightarrow n\pi_g$ Rydberg series) or some related explanation that is responsible for this underestimate of the $2\sigma_u \rightarrow k\pi_g$ oscillator strength. This bears further study but is beyond the scope of the current investigation. It is examined in greater detail in a related alignment study performed via fluorescence polarization measurements.[85] Alignment studies naturally separate continua of alternative symmetries (i.e., $k\pi_g$ vs $k\sigma_g$),[81,82] whereas rotational distributions do not. A more complete discussion is given in Ref. 85.

The partial wave composition of the photoelectron matrix element is shown for the 4σ level of CO in Fig. 13. Specifically, there is an intense $l=3$ shape resonance in the $4\sigma \rightarrow k\sigma$ continuum, which is the main contribution. In addition, there is a broad enhancement in the $l=3$ component for the $4\sigma \rightarrow k\pi$ continuum at lower energies, which further contributes to the large ΔN transitions at low energy. Analysis of the eigenphase sum indicates that this $4\sigma \rightarrow k\pi$ feature is nonresonant, whereas the $4\sigma \rightarrow k\sigma$ continuum shows an increase of about π radians in the eigenphase sum in the region of the $l=3$ peak, consistent with shape-resonant behavior. These $l=3$ components enhance large ΔN transitions in the low energy region. As the photon energy is increased, other high-l components grow in strength, sustaining the large ΔN transitions observed at lower energy and resulting in comparatively flat rotational distributions as a function of energy. While the agreement between experiment and theory is reasonably good, it is apparent that theory somewhat overestimates the influence of the shape resonance on the rotational distributions. Polarization measurements indicate that the calculations overestimate the contribution of the $l=3$ component in the $4\sigma \rightarrow k\sigma$ continuum. This is discussed in greater detail elsewhere.[84,85]

It is interesting to consider the influence that symmetry has on the behavior of the N_2 and CO ion distributions. Although these systems are valence isoelectronic and chemically similar in many respects, symmetry is responsible for one of the features that makes the results in Figs. 7 and 8 so qualitatively different. The shape resonant $l=3$ wave in CO $(4\sigma^{-1})$ photoionization which is responsible for large ΔN transitions at low energy has no counterpart in N_2 $(2\sigma_u^{-1})$ photoionization, as only even l components are possible. On the other hand, it is not clear why there are no significant Cooper minima in the CO $(4\sigma \rightarrow k\sigma)$ channel as one may expect in analogy with the $2\sigma_u \rightarrow k\sigma_g$ channel of N_2.

C. Is there limiting behavior at high energy?

The changing N_2^+ $(B\ ^2\Sigma_u^+)$ distributions at such high energies (i.e., $E_K \geqslant 200$ eV) motivate a simple question. Namely, is there a high-energy limiting behavior for rotational excitation in molecular photoionization? It seems natural to assume that beyond a certain energy the electron may no longer ''feel'' the influence of the molecular potential, implying that the rotational distributions should approach a limiting behavior. In order to evaluate the high-energy trends in more detail, we extended the calculations of the N_2^+ $(B\ ^2\Sigma_u^+)$ rotational populations to $h\nu_{\text{exc}}=600$ eV and the results are shown in Fig. 14. They clearly indicate that the rotational distributions continue to change with larger ΔN transitions growing as the energy increases. In fact, it appears that there is another inflection point in the population curves at $h\nu_{\text{exc}} \approx 300$ eV. By the time that the photon energy exceeds 500 eV, the dominant transitions are $\Delta N \geqslant 5$. This absence of limiting behavior highlights the molecular nature of the photoionization dynamics, which persist to the highest energies. The implication is that attempts to treat the scatter-

ing dynamics with model potentials must be done with great care, *even far above threshold*. Models which do not treat the molecular potential realistically can oversimplify the photoelectron dynamics and will not properly account for the physical aspects of the scattering.

Experiments attempting to reach energies near the upper limits shown in Fig. 14 are difficult, as two obstacles interfere. First, the cross sections are decreasing monotonically with increasing energy, so even in the absence of competing processes, the intensities become vanishingly small beyond $h\nu_{\mathrm{exc}} \geqslant 250$ eV. Second, there are competing processes that complicate fluorescence studies of $2\sigma_u^{-1}$ photoionization of N_2 at energies above 400 eV.[92–94] At these energies, the N_2 $1s$ electron is excited into either autoionizing orbitals or the continuum. It has been shown that these core-hole states can decay to form the $2\sigma_u^{-1}$ valence hole state, which then fluoresces. We are currently investigating the mechanism responsible for this core–hole decay[94] and it is clear that such processes will dominate signals coming directly from the $2\sigma_u$ valence electron ejection. This interfering process may represent an opportunity, as opposed to being viewed solely as the limit for which direct valence electron ejection studies are possible. Specifically, related core–electron ejection processes may be amenable to study by exploiting valence–hole fluorescence detection, as has been discussed elsewhere.[47,92,93]

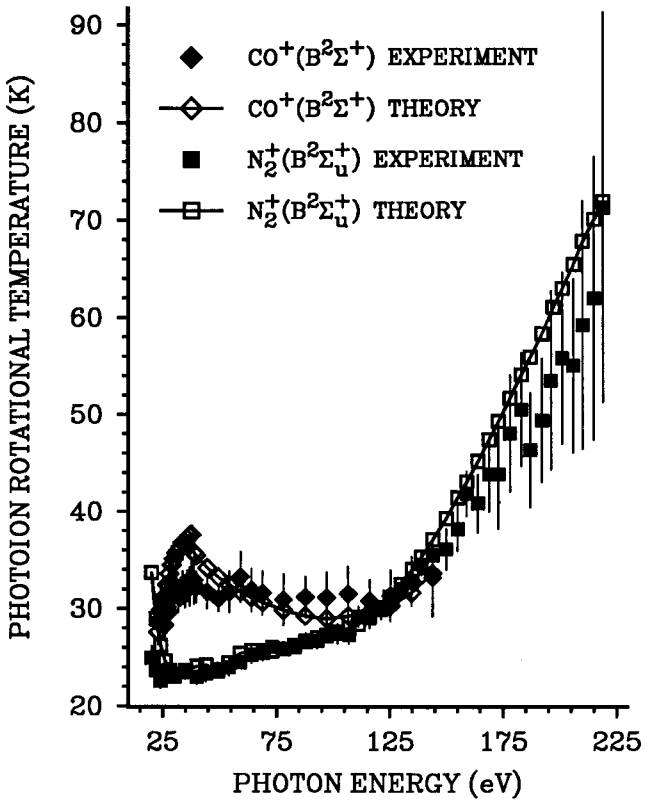

FIG. 15. Comparison of rotational temperature of excited state ions. Note the growth of high-N levels at higher energies. This indicates that larger ΔN grow in intensity with energy and that there is apparently no high-energy limit.

D. Implications for electron beam diagnostics of supersonic expansions

Another aspect of the data which bears scrutiny is a comparison between our photoionization results of rotational excitation and previous electron impact studies. There have been many investigations of electron impact ionization of N_2.[86,87,95–99] A primary goal in such studies has been to assess the suitability of electron impact ionization as a means of estimating the rotational temperature of supersonic expansions. This has been a topic of intense interest in its own right, as supersonic expansions have widely enabled spectroscopic and dynamical studies in modern chemical physics.[100,101] Fluorescence from electronically excited ions created via electron impact is a simple means of obtaining rotationally resolved data and it was hoped that an electron impact probe could be used to evaluate the rotational distribution of the neutral target gas expanded in the supersonic expansion.[86] However, relating the rotational distributions of the ions formed via electron impact with the nascent neutral rotational distributions required unsubstantiated assumptions regarding the rotational excitation that occurs in the ionization step. The ion rotational distributions were observed to level out at impact energies greater than 100 eV. The initial attempts to interpret such data relied on the assumption of atomiclike behavior, resulting in $\Delta N = \pm 1$ transitions at higher energy.[86] Our present results show that such behavior is not even approximately true for either the N_2 or CO cases and that more detailed calculations are required in order to employ electron impact ionization as a means of interrogating rotational distributions of molecules formed in supersonic expansions. While not the main motivation for the current investigation, the comparison of electron and photon impact results is interesting and we digress briefly to describe them.

Previous electron impact investigations characterized the ionic distributions using rotational temperature as a parameter and assumed that a limiting behavior was reached at higher energy and that similar behavior might be expected optically at some energies. As we have seen, a high energy limit is not reached optically and it is instructive to recast the N_2^+ $(B\ ^2\Sigma_u^+)$ and CO^+ $(B\ ^2\Sigma^+)$ data in terms of effective rotational temperatures. In order to fit the observed populations to rotational temperatures, we use procedures described elsewhere.[37] The results of fitting the data to temperatures for the excited state ions are shown in Fig. 15. The theoretical population distributions are also fitted to rotational temperatures using the same procedures and the comparison with experiment is excellent. We note that the error bars shown in Fig. 15 are large at high energy because a Boltzmann distribution does not fit the data well, not because the counting statistics are much poorer for the high energy data.

Figure 15 illustrates three points clearly. First, N_2 does not have a high energy limit and its low energy behavior shows a considerable excursion in its own right. Second, CO and N_2 have qualitatively different dependences at both high and low energies, indicating that a general (closed-form) formulation for extracting initial neutral distributions is not possible. Third, while this may appear to be a pessimistic assess-

ment for using electron impact ionization as a means of determining molecular beam characteristics, there is actually a constructive conclusion to be drawn from Fig. 15. The excellent agreement between the photon impact experiment and theory indicates that theory is capable of inverting observed electron impact ionization data and obtaining neutral rotational distributions. The calculations required for comparison with electron impact data at high energies are straightforward and are very closely related to the photon impact calculations.[77] Modern advances in the theory of fundamental scattering dynamics can enable electron scattering to fulfill the role originally envisioned by previous investigators[86,87,95–99] as a means of diagnosing molecular beam expansion characteristics. We will describe the application of photon and electron impact ionization as a diagnostic tool in detail elsewhere.[102]

E. Sensitivity of analysis to initial temperature

The comparison between experiment and theory is excellent and indicates that the results and interpretation are meaningful. However, there is one adjustable parameter used in generating these comparisons, namely, the rotational temperature of the neutral target gas. It is worthwhile to examine how the comparison between experiment and theory changes with the assumed target rotational temperature. This permits us to determine how sensitive the interpretation is to an adjustable parameter. This can be evaluated from Fig. 16, which shows comparisons of theory with experiments for three different target rotational temperatures of 10, 14, and 18 K. The comparisons clearly show that 14 K results give the best fit to the data and, hence, we have presented theoretical results based on an assumed 14 K rotational temperature. However, it is important to note that the qualitative trends observed in these comparisons are indistinguishable for all three initial temperature assumptions. As a result, qualitative aspects of the conclusions are unaffected by the assumptions regarding the initial target temperature.

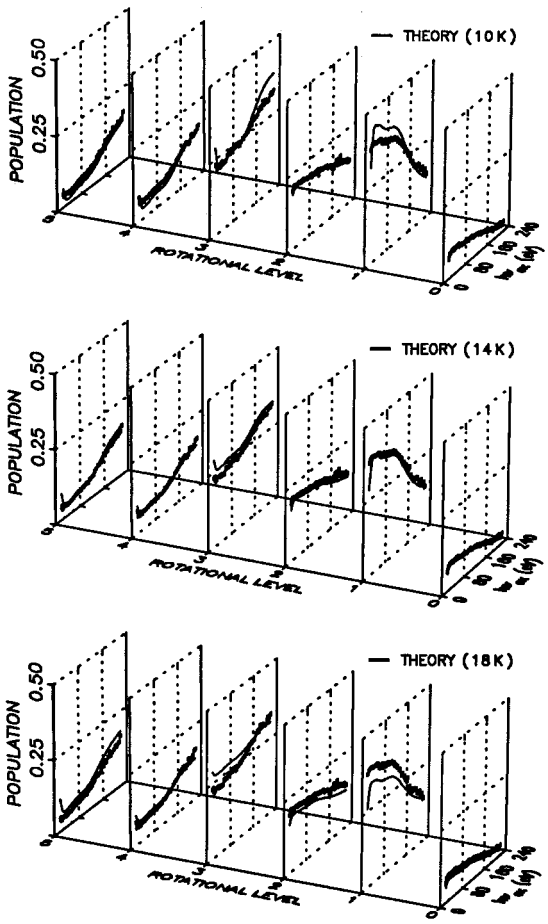

FIG. 16. N_2 results calculated for different initial temperatures. Note that the sensitivity to initial temperature is not pronounced and does not affect the qualitative trends observed.

V. SUMMARY

The primary goal of this study has been to investigate the relationship between photoelectron energy and photoion rotation. This aim has been largely realized. In particular, the strategy of exploiting dispersed fluorescence from photoions significantly expands the range of possible studies into photoionization dynamics. While previous studies of photoion rotation have been limited to threshold or near-threshold ionization, the present studies extend to more than 200 eV and this increase of 2 orders of magnitude allows us to study the systematics of shape resonances and Cooper minima, which are ubiquitous for molecular systems. The extension of the spectral range comes at the price of state-specific information on the target molecule but this limitation does not unduly restrict the information content of the measurements, particularly when theory and experiment work together to assess the trends in detail. Thus these results demonstrate that rotationally resolved photoion fluorescence complements existing laser-based photoelectron and induced fluorescence methods.

By covering such broad spectral ranges, these studies can survey the trends that help characterize molecular photoionization dynamics. In particular, the qualitatively different behavior of N_2 and CO underscores the chemical sensitivity of rotational excitation in photoionization. The N_2 results demonstrate that $\Delta N=\pm 3$ transitions grow in intensity relative to the $\Delta N=\pm 1$ transitions at high photoelectron kinetic energies and the inflection point at $h\nu_{\mathrm{exc}}\approx 120$ eV in the population curves is due to Cooper minima in the $2\sigma_u \rightarrow k\sigma_g$ channel. The CO rotational populations are very flat in comparison to the N_2 curves. Theory shows that the flat rotational populations for CO^+ ($B\ ^2\Sigma^+$) are due to large ΔN transitions occurring at both high and low energies. The large ΔN transitions occurring at low energy are due to an $l=3$ shape resonance in the $4\sigma \rightarrow k\sigma$ channel. This shape resonance with its $l=3$ dominant component sustains high ΔN transitions, even at low photon energy ($h\nu_{\mathrm{exc}}\approx 35$ eV). The differences in CO and N_2 are dramatic and the coverage of a large range by the fluorescence measurements provides new perspectives and opportunities for studies of molecular photoionization dynamics.

In closing, we restate the primary messages from this study. First, the dramatic differences between N_2 and CO highlight the role of the molecular ion as an electron lens that

the photoelectron must traverse. Both chemically and physically useful information can be derived from such a viewpoint and the ability to study energy-dependent aspects deep into ionization continua makes it possible to study entirely new aspects of the ionization dynamics. Second, we have demonstrated that probing molecular aspects of the ionization dynamics, such as rotation, provides a unique and powerful view into the scattering of the photoelectron by the molecular ion. While quantities that parallel atomic parameters are useful in their own right (vibrationally resolved asymmetry parameters and cross sections), studies which resolve molecular motion add a new and useful perspective. Third, highly resolved photoionization studies have significant implications for studies in other areas. As an example, we note that the application of electron beam ionization of molecular beams can provide information on the neutral rotational distribution only when microscopic details of the ionization dynamics are known. There are serious pitfalls in oversimplifying the ionization process and this has significant implications for electron bombardment ionization as a probe of molecular beam rotational distributions.[102] Finally, these results show that the dispersed fluorescence method provides us with an ideal means of probing photoionization dynamics both near and far from the ionization threshold. Such capabilities afford us with the opportunity to explore new facets regarding the correlation of electronic and nuclear degrees of freedom in chemical physics.

ACKNOWLEDGMENTS

The efforts of the CAMD staff are greatly appreciated and we are particularly indebted to Dr. Volker Saile, Dr. John Scott, and Dr. Eizi Morikawa for their support with the plane grating monochromator. We are also indebted to Professor Roger Stockbauer for many helpful discussions. E.D.P. acknowledges support from NSF (CHE-9315857) and the Louisiana LEQSF program. Work at the California Institute of Technology was supported by grants from the Air Force Office of Scientific Research and the Office of Health and Environmental Research of the U.S. Department of Energy. We also acknowledge use of resources of the Jet Propulsion Laboratory/Caltech Cray Y-MP2E/232 Supercomputer.

[1] L. Äsbrink, Chem. Phys. Lett. **7**, 549 (1970).
[2] A. D. Buckingham, B. J. Orr, and J. M. Sichel, Philos. Trans. R. Soc. London Sect. A **268**, 147 (1970).
[3] D. Dill, Phys. Rev. A **6**, 160 (1972).
[4] J. E. Pollard, D. J. Trevor, J. E. Reutt, Y. T. Lee, and D. A. Shirley, J. Chem. Phys. **77**, 34 (1982).
[5] S. T. Pratt, P. M. Dehmer, and J. L. Dehmer, J. Chem. Phys. **78**, 4315 (1983).
[6] W. G. Wilson, K. S. Viswanathan, E. Sekreta, and J. P. Reilly, J. Phys. Chem. **88**, 672 (1984).
[7] C. H. Greene and Ch. Jungen, Adv. At. Mol. Phys. **21**, 51 (1985).
[8] E. D. Poliakoff, J. C. K. Chan, and M. G. White, J. Chem. Phys. **85**, 6232 (1986).
[9] S. N. Dixit and V. McKoy, Chem. Phys. Lett. **128**, 49 (1986).
[10] R. G. Tonkyn, J. W. Winniczek, and M. G. White, Chem. Phys. Lett. **164**, 137 (1989).
[11] J. Xie and R. N. Zare, Chem. Phys. Lett. **159**, 399 (1989).
[12] H. Lefebvre-Brion, Chem. Phys. Lett. **171**, 377 (1990).
[13] M. S. Child and Ch. Jungen, J. Chem. Phys. **93**, 7756 (1990).
[14] R. D. Gilbert and M. S. Child, Chem. Phys. Lett. **187**, 153 (1991).
[15] K. Müller-Dethlefs and E. W. Schlag, Annu. Rev. Phys. Chem. **42**, 109 (1991).
[16] F. Merkt and T. P. Softley, J. Chem. Phys. **96**, 4149 (1992).
[17] G. P. Bryant, Y. Jiang, M. Martin, and E. R. Grant, J. Phys. Chem. **96**, 6875 (1992).
[18] W. Kong, D. Rodgers, J. W. Hepburn, K. Wang, and V. McKoy, J. Chem. Phys. **99**, 3159 (1993).
[19] R. T. Wiedmann, M. G. White, K. Wang, and V. McKoy, J. Chem. Phys. **100**, 4738 (1994).
[20] J. A. Blush, P. C. Chen, R. T. Wiedmann, and M. G. White, J. Chem. Phys. **98**, 3557 (1993).
[21] I. Fischer, A. Lochschmidt, A. Strobel, G. Niedner-Schatteburg, K. Müller-Dethlefs, and V. Bondybey, J. Chem. Phys. **94**, 3592 (1993).
[22] K. Wang and V. McKoy, J. Chem. Phys. **95**, 4977 (1991).
[23] J. L. Dehmer, D. Dill, and A. C. Parr, in *Photophysics and Photochemistry in the Vacuum Ultraviolet*, edited by S. P. McGlynn, G. L. Findley, and R. H. Heubner (Reidel, Dordrecht, Holland, 1985), p. 341.
[24] J. L. Dehmer, A. C. Parr, and S. H. Southworth, in *Handbook on Synchrotron Radiation*, edited by G. V. Marr (North-Holland, Amsterdam, 1987), Vol. II.
[25] P. W. Langhoff, in *Resonances in Electron-Molecule Scattering, van der Waals Complexes and Reactive Chemical Dynamics*, edited by D. G. Truhlar, ACS Symp. Ser. No. 263 (American Chemical Society, Washington, DC, 1984).
[26] J. W. Gallagher, C. E. Brion, J. A. R. Samson, and P. W. Langhoff, J. Chem. Phys. Ref. Data **17**, 9 (1988).
[27] J. W. Cooper, Phys. Rev. **128**, 681 (1962).
[28] S. T. Manson and J. W. Cooper, Phys. Rev. **165**, 126 (1968).
[29] H. C. Choi, R. M. Rao, A. G. Mihill, S. Kakar, E. D. Poliakoff, K. Wang, and V. McKoy, Phys. Rev. Lett. **72**, 44 (1994).
[30] E. D. Poliakoff, Chem. Rev. (to be published).
[31] E. D. Poliakoff, in *Vacuum Ultraviolet Photoionization and Photodissociation of Molecules and Clusters*, edited by C. Y. Ng (World Scientific, Singapore, 1991).
[32] E. D. Poliakoff, S. Kakar, and R. A. Rosenberg, J. Chem. Phys. **96**, 2740 (1992).
[33] K. Wang and V. McKoy, J. Chem. Phys. **95**, 7872 (1991).
[34] K. S. Viswanathan, E. Sekreta, E. R. Davidson, and J. P. Reilly, J. Phys. Chem. **90**, 5078 (1986).
[35] K. S. Viswanathan, E. Sekreta, and J. P. Reilly, J. Phys. Chem. **90**, 5658 (1986).
[36] X. Song, E. Sekreta, J. P. Reilly, H. Rudolph, and V. McKoy, J. Chem. Phys. **91**, 6062 (1989).
[37] S. Kakar, H. C. Choi, and E. D. Poliakoff, J. Chem. Phys. **97**, 6998 (1992).
[38] H. Rudolph and V. McKoy, J. Chem. Phys. **91**, 2235 (1989).
[39] K. Wang, J. A. Stephens, and V. McKoy, J. Chem. Phys. **95**, 6456 (1991).
[40] M. Braunstein, V. McKoy, S. N. Dixit, R. G. Tonkyn, and M. G. White, J. Chem. Phys. **93**, 5345 (1990).
[41] E. de Beer, M. Born, C. A. de Lange, and N. P. C. Westwood, Chem. Phys. Lett. **186**, 40 (1991).
[42] E. de Beer, M. P. Koopmans, C. A. de Lange, Y. Wang, and W. A. Chupka, J. Chem. Phys. **94**, 7634 (1991).
[43] E. de Beer, C. A. de Lange, J. A. Stephens, K. Wang, and V. McKoy, J. Chem. Phys. **95**, 714 (1991).
[44] W. A. Chupka, J. Chem. Phys. **98**, 4520 (1992).
[45] K. L. Reid, D. J. Leahy, and R. N. Zare, Phys. Rev. Lett. **68**, 3527 (1992).
[46] S. W. Allendorf, D. J. Leahy, D. C. Jacobs, and R. N. Zare, J. Chem. Phys. **91**, 2216 (1989).
[47] M. Mahalingam, K. Lee, and D. M. Hanson, J. Chem. Phys. **98**, 5239 (1993).
[48] K. J. Randall, A. L. D. Kilcoyne, H. M. Köppe, J. Feldhau, A. M. Bradshaw, J. E. Rubensson, W. Eberhardt, Z. Xu, P. D. Johnson, and Y. Ma, Phys. Rev. Lett. **71**, 1156 (1993).
[49] C. T. Chen, Y. Ma, and F. Sette, Phys. Rev. A **40**, 6737 (1989).
[50] J. D. Bozek, G. M. Bancroft, J. N. Cutler, and K. H. Tan, Phys. Rev. Lett. **65**, 2757 (1990).
[51] A. Niehaus and M. W. Ruf, Chem. Phys. Lett. **11**, 55 (1971).
[52] P. Baltzer, L. Karlsson, and B. Wannberg, Phys. Rev. A **46**, 315 (1992).
[53] M. G. White, in *Highly Resolved Laser Photoionization and Photoelectron Studies*, edited by I. Powis (Wiley, New York, 1995).
[54] K. Müller-Dethlefs, in *Highly Resolved Laser Photoionization and Photoelectron Studies*, edited by I. Powis (Wiley, New York, 1995).
[55] E. R. Grant, in *Highly Resolved Laser Photoionization and Photoelectron Studies*, edited by I. Powis (Wiley, New York, 1995).

[56] T. P. Softley, in *Highly Resolved Laser Photoionization and Photoelectron Studies*, edited by I. Powis (Wiley, New York, 1995).
[57] K. Wang, J. A. Stephens, and V. McKoy, J. Phys. Chem. **97**, 9874 (1993).
[58] R. T. Wiedmann, M. G. White, K. Wang, and V. McKoy, J. Chem. Phys. **98**, 7673 (1993).
[59] A. Strobel, I. Fischer, J. Staeker, G. Nieder-Schatteburg, K. Müller-Dethlefs, and V. Bondybey, J. Chem. Phys. **97**, 2332 (1991).
[60] E. R. Grant and M. G. White, Nature (London) **354**, 249 (1991).
[61] M.-T. Lee, K. Wang, V. McKoy, R. G. Tonkyn, R. T. Wiedmann, E. R. Grant, and M. G. White, J. Chem. Phys. **96**, 7848 (1992).
[62] X. Zhang, J. M. Smith, and J. L. Knee, J. Chem. Phys. **99**, 3133 (1993).
[63] T. Baumert, R. Thalweiser, and G. Gerber, Chem. Phys. Lett. **209**, 29 (1993).
[64] J. Harrington and J. C. Weisshaar, J. Chem. Phys. **97**, 2809 (1992).
[65] E. D. Poliakoff, M.-H. Ho, G. E. Leroi, and M. G. White, J. Chem. Phys. **84**, 4779 (1986).
[66] E. D. Poliakoff, M.-H. Ho, M. G. White, and G. E. Leroi, Chem. Phys. Lett. **130**, 91 (1986).
[67] L. A. Kelly, L. Duffy, B. Space, E. D. Poliakoff, M. G. White, S. H. Southworth, and P. Roy, J. Chem. Phys. **90**, 1544 (1989).
[68] S. Kakar, H. C. Choi, and E. D. Poliakoff, Chem. Phys. Lett. **190**, 489 (1992).
[69] S. Kakar, H. C. Choi, and E. D. Poliakoff, J. Chem. Phys. **97**, 4690 (1992).
[70] S. Kakar, E. D. Poliakoff, and R. A. Rosenberg, J. Chem. Phys. **96**, 23 (1992).
[71] B. C. Craft, M. Feldman, E. Morikawa, E. D. Poliakoff, V. Saile, J. D. Scott, and R. L. Stockbauer, Rev. Sci. Instrum. **63**, 1561 (1992).
[72] E. Morikawa, J. D. Scott, E. D. Poliakoff, R. L. Stockbauer, and V. Saile, Rev. Sci. Instrum. **63**, 1300 (1992).
[73] D. H. Levy, Ann. Rev. Phys. Chem. **31**, 197 (1980).
[74] K. Wang and V. McKoy, in *Highly Resolved Laser Photoionization and Photoelectron Studies*, edited by I. Powis (Wiley, New York, 1995).
[75] A. R. Edmonds, *Angular Momentum in Quantum Mechanics* (Princeton University, Princeton, 1974).
[76] M. Braunstein, V. McKoy, and S. N. Dixit, J. Chem. Phys. **96**, 5726 (1992).
[77] R. R. Lucchese, K. Takatsuka, and V. McKoy, Phys. Rep. **131**, 147 (1986).
[78] R. R. Lucchese, G. Raseev, and V. McKoy, Phys. Rev. A **25**, 2572 (1982).
[79] H. C. Choi, Ph.D. thesis, Louisiana State University.
[80] G. Herzberg, in *Molecular Spectra and Molecular Structure, I. Spectra of Diatomic Molecules* (Krieger, Malabar, FL, 1989).
[81] E. D. Poliakoff, J. L. Dehmer, D. Dill, A. C. Parr, K. H. Jackson, and R. N. Zare, Phys. Rev. Lett. **46**, 907 (1981).
[82] J. A. Guest, K. H. Jackson, and R. N. Zare, Phys. Rev. A **28**, 2217 (1983).
[83] J. A. Guest, M. A. O'Halloran, and R. N. Zare, J. Chem. Phys. **81**, 2689 (1984).
[84] R. Das, C. Wu, A. G. Mihill, E. D. Poliakoff, K. Wang, and V. McKoy, J. Chem. Phys. **101**, 5402 (1994).
[85] R. Das, C. Wu, A. G. Mihill, E. D. Poliakoff, K. Wang, and V. McKoy, J. Phys. Chem. **99**, 1741 (1995).
[86] E. P. Muntz, Phys. Fluids **5**, 80 (1962).
[87] B. M. DeKoven, D. H. Levy, H. H. Harris, B. R. Zegarski, and T. A. Miller, J. Chem. Phys. **74**, 5659 (1981).
[88] J. Kreile, A. Schweig, and W. Thiel, Chem. Phys. Lett. **108**, 259 (1984).
[89] A. Hamnett, W. Stoll, and C. E. Brion, J. Electron. Spectrosc. **8**, 367 (1976); E. W. Plummer, T. Gustafsson, W. Gudat, and D. E. Eastman, Phys. Rev. A **15**, 2339 (1977).
[90] J. Davenport, Phys. Rev. Lett. **36**, 945 (1976).
[91] D. Dill and J. L. Dehmer, J. Chem. Phys. **61**, 692 (1974); S. Wallace, D. Dill, and J. L. Dehmer, J. Phys. B **12**, L417 (1979); J. L. Dehmer, D. Dill, and S. Wallace, Phys. Rev. Lett. **43**, 1005 (1979).
[92] E. D. Poliakoff, B. Space, L. A. Kelly, L. Duffy, M. G. White, S. H. Southworth, and P. Roy, J. Chem. Phys. **89**, 4048 (1988).
[93] E. D. Poliakoff, B. Space, L. A. Kelly, L. Duffy, M. G. White, S. H. Southworth, and P. Roy, Chem. Phys. **129**, 65 (1989).
[94] R. M. Rao, J. Wu, and E. D. Poliakoff (to be published).
[95] I. Tokue, A. Masuda, H. Kume, and Y. Ito, Chem. Phys. **158**, 161 (1991).
[96] S. P. Hernandez, P. J. Dagdigian, and J. P. Doering, Chem. Phys. Lett. **91**, 409 (1982); J. Chem. Phys. **77**, 6021 (1982); P. J. Dagdigian and J. P. Doering, **78**, 1846 (1983).
[97] H. Helvajian, B. M. DeKoven, and A. P. Baronavski, Chem. Phys. **90**, 175 (1984).
[98] P. W. Zetner, M. Darrach, P. Hammond, W. B. Weterveld, R. L. McConkey, and J. W. McConkey, Chem. Phys. **124**, 453 (1988).
[99] A. Nakajima, T. Nagata, T. Kondow, and K. Kuchitsu, Chem. Phys. Lett. **151**, 511 (1988).
[100] See, for example, *Atomic and Molecular Beam Methods*, edited by G. Scoles (Oxford University, New York, 1988), Vol. 1, and references therein.
[101] P. C. Engelking, Chem. Rev. **91**, 399 (1991).
[102] E. D. Poliakoff, R. M. Rao, A. G. Mihill, K. Wang, and V. McKoy (to be published).